

Large-scale parameter modelling for millimeter-wave multiple-input multiple-output channel in 5G ultra-dense network

Olabode Idowu-Bismark, Francis Idachaba, Aderemi A. Atayero

Department Electrical and Information Engineering, Covenant University, Ota Ogun State, Nigeria

Article Info

Article history:

Received May 10, 2021

Revised Mar 4, 2022

Accepted Mar 16, 2022

Keywords:

3D channel modelling

5G

Angular spread

Delay spread

MIMO

ABSTRACT

Network densification (ND) in 5G has been suggested as a solution to improve network capacity. ND has small cell backhaul as its bottleneck in the ensuing ultra-dense network (UDN). Due to the new deployment scenarios of small cells, it becomes necessary to thoroughly investigate the radio-propagation characteristics of the new transmission path between the base station and the small cells. The problem of the impact of small cell height on the backhaul large-scale parameters under typical outdoor-to-indoor (high-rise) and outdoor-to-outdoor (street canyon) scenarios was first investigated. Next, the probability distribution functions of the various parameters were investigated and modeled. Novel use of 5G NR air interface using a deterministic ray-tracing engine to characterize the backhaul at 28 GHz center frequency and 100 MHz bandwidth using 4x4 cross-polarized uniform planar array (UPA) at the base station and 2x2 multiple input, multiple output (MIMO) antennas at the small cells was proposed. New sets of models for root mean square (RMS) delay spread and RMS angular spread suitable for predicting network deployment in the two scenarios and similar environments were presented.

This is an open access article under the [CC BY-SA](https://creativecommons.org/licenses/by-sa/4.0/) license.



Corresponding Author:

Olabode Idowu-Bismark

Department of Electrical and Information Engineering, Covenant University

Cannan Land, Ota Ogun State, Nigeria

Email: idowubismarkolabode@gmail.com

1. INTRODUCTION

The explosive ever increasing demand for mobile traffic as a result of everyone's desire for online presence such as Facebook, Twitter, YouTube and video streaming [1] among others has placed the long term evolution (LTE) system under pressure [2], leading to the need for the proposed 5G network [3]. It has been suggested in [4] that network densification is a method to achieve the requirement of 5G. This will lead to enhanced capacity of the network, improvement in terms of coverage as well as energy efficiency improvement. Meanwhile, urban networks are not flat since we have various heights of buildings and structures dotting the landscape. Therefore, the current stochastic geometry way of considering all base stations and user equipment (UE) as existing only on a 2D plane according to [4] is erroneous. In the forthcoming 5G deployment, it is expected that small cells (SC) such as picocells and femtocells will be placed indoor for the internet of things (IoT) traffic evacuation, as well as other indoor data traffic as 80% of data traffic, are used indoor [5]. The consequences of the above on the communication environment will be intense as many more SCs and UEs will be used in complex 3D topological urban environments for which most of the current multiple input, multiple output (MIMO) channel models cannot handle since they do not consider 3D channel parameters such as the elevation angles and the 3D angular spread. The above ability to communicate with UE in 3D topological urban environments will be made possible with the use of a full

dimension MIMO communication system employing 3D beamforming (3DBF) in 5G [6]. 3DBF novel method of improving system performance unearth completely new challenges requiring pressing attention such as developing precise 3D channel models, performance prediction, and analysis to account for the impact of the channel parameters in the elevation domain. The classical sub-6 GHz channel models are geometry-based stochastic channel models (GSCMs) [7] and are based on a base station to user equipment (BS-UE) link type. However, current mmWave channel models have not only included the inherent characteristics of the mmWave channels but have also added channel properties for 5G communication technologies, such as massive MIMO, spatial consistency, and beamforming [8] which unfortunately the GSCMs models cannot do due to their lack of channel measurement campaigns for various 5G link types [9].

Map-based mmWave channel models that exploit ray-tracing (RT) have come of age. They serve as a way to model the irregular layouts of small cells and to support new applications' link types, including device-to-device (D2D), and vehicle-to-everything (V2X) [10]. RT is typically used to evaluate hardware testbeds [11] and also to authenticate the theoretical performance of vital 5G technologies [12]. Many mmWave channel models have also adopted RT techniques or map-based models, those include, New York University simulation (NYUSIM) model developed by the NYU wireless group where hardware channel measurements were complemented with RT [13]. Also, the METIS group model has a map-based channel model that supports the various 5G modeling requirements [14]. The use of RT, map-based modeling for 5G mmWave communication systems was introduced to overcome the shortcomings of the classical GSCM models [8]. This is the motivation for this present study where we use REMCOM wireless insite RT, a map-based simulation engine to characterized the backhaul links of small cells in UDN and extract the channel large scale parameters to produce new sets of models for a street canyon and high-rise scenarios suitable for network deployment. To support multiple stream point-to-multipoint backhaul link where mmWave MIMO takes advantage of beamforming and spatial multiplexing techniques to concurrently support multiple SC BSs, Gao *et al.* [15] and Xia *et al.* [16] has carried out work to investigate the characteristics of mmWave MIMO channel parameters and how they impact on various capabilities of the wireless channel including the channel capacity. According to Gao *et al.* [15], the authors suggested the use of mmWave MIMO for enhanced link reliability. The paper did not deal with mmWave MIMO channel characterization but laid the foundation for the use in SC BS backhaul. Xia *et al.* [16] used generative neural networks to train obtained data and model the millimeter-wave channel parameter in line of sight (LOS) and non-line of sight (NLOS) situations. In the work of Almesaeed *et al.* [17] where the need for user-specific elevation beamforming and full-dimensional MIMO is emphasized for increased network capacity, it was stated that the characterization of the channel elevation angles and other elevation related statistics such as elevation spread and distribution as well as the power elevation spectrum should be characterized for FD-MIMO and 3D elevation beamforming performance analysis. This paper then reviewed the use of these channel parameters in the design of 3D channel models. However, those parameters were not modeled. Yang *et al.* [18] investigated the impact of vehicle obstructions on the angular distributions of multipath components. Alsharif *et al.* [19] evaluated the effect of 5G small cell systems on the energy efficiency (EE) in a 5G cellular system using the large-scale parameters of pathloss and shadowing both of which affect the small cells received signal strength. They concluded that massive MIMO in the mmWave system improves the EE of small cells in UDN while reducing interference. Zheng *et al.* [20] researched the impact of receiver antenna height rather than the impact of microcell BS antenna height and also, the authors use channel measurements and the space-alternating generalized expectation-maximization (SAGE) algorithm to extract the channel parameters.

In the above review, to the best of our knowledge, no single paper considered or performed an extensive study and compared the two scenarios under consideration here. While studies were carried out in various locations, no paper to the best of our knowledge is written to consider such studies in an urban propagation environment of Lagos Nigeria. Due to the new deployment scenarios of small cells, it becomes necessary to thoroughly investigate the radio-propagation characteristics of the new transmission path between the base station and the small cells. In this research work, we first investigate the problem of the impact of small cell height on the channel large-scale parameters of RMS delay spread and the RMS angular spread under typical outdoor-to-indoor (high-rise) and outdoor-to-outdoor (street canyon) scenarios. The distribution of the various parameters under the new deployment was investigated and their probability distribution functions modeled. We propose a novel use of 5G new radio (5G NR) air interface using deterministic wireless insite ray tracing engine and 3D map of urban areas of Lagos Island, Lagos State, Nigeria to characterize and extract the large-scale parameter dataset of the backhaul link. We model the RMS delay spread and the RMS angular spread for the new deployment scenarios. The summary of the contributions of this paper is the development of a new series of models suitable for predicting network deployment in an urban microcell (UMi) street canyon and high-rise scenarios in Lagos Island, Nigeria, and a similar environment. The rest of the paper is arranged as shown in; Section 2 considered the research method and simulation setup while section 3 present the result and discussions. We conclude in section 4.

2. RESEARCH METHOD AND SIMULATION SETUP

In this work, we propose the use of a 5G new radio (5G NR) air interface where we employ closed-loop diversity in the form of maximum ratio transmission-maximum ratio combining (MRT-MRC) to provide optimal performance reference against wireless fading. We use adaptive modulation to improve the spectral efficiency and to provides guaranteed capacity and service availability by increasing or decreasing the modulation rate. Using the REMCOM Wireless Insite ray tracing engine and a digital map of Lagos Island, we simulated a UDN backhaul link with small cells in a street canyon and high-rise environment. The small cells in the high-rise scenario are located 1 per floor on the 30 floors of a 30-story building in Lagos Island, Nigeria with a 3.5 m spacing on floor-by-floor (vertical spacing) giving a total of 105 m building height. This gives us a total of 30 receivers for this scenario. For the street canyon scenario, the small cell receivers are located along a route on Broad Street Lagos at a height of 2.5m and 1m spacing along the street (for spatial consistency). The street is about 14-meter width with low to high-rise buildings on both sides. The street also has narrow and wider feeder streets on both sides. The total number of the small cell is 596 thus covering a length of 596 m. Table 1 shows the simulation parameters and their values.

Table 1. Table of simulation parameters

Simulation Parameters	Values
Number of street small cells	596
Number of high-rise small cells	30
Carrier Frequency	28 GHz
Bandwidth	100 MHz
BS Transmit power	30 dBm
BS height	10m
Street Small cell height	2.5m
High-rise Small cell height	various
Distance of High-rise Building from BS	238m
BS Antenna	4 x 4 UPA
Small cell antenna	2 x 2
Antenna element spacing	1 wavelength

3. RESULTS AND DISCUSSION

After the completion of the simulations for the various scenarios and the extraction of the various dataset. The dataset is then exported into MATLAB 2017b for post-processing and modeling. To have a statistical distribution that best describes the dataset of our variables (channel parameters), we estimated the unknown parameters of the many distributions using the maximum likelihood estimation (MLE) where the best relationships are then selected using the Akaike information criterion (AIC).

3.1. RMS delay spread

The rms delay spread relationship with distance was first determined and modeled. The pdf distribution was then determined and the mean and standard variation extracted for both scenarios. The distance dependency model is shown in section 3.1.1 while the pdf distribution is shown in section 3.1.2.

3.1.1. RMS delay spread distance dependency

Modeling the root mean square (RMS) DS distance dependency (DD) for a distance up to 200 m in the street canyon scenario, we see a linear relationship as depicted by the fitted polynomial of the first-degree curve in Figure 1 where RMS DS increases linearly as distance increases. This is evidence in the fact that we are considering a street canyon environment that behaves like a waveguide to the transmitted signal. The effect of this is that all the arriving multipath components are from the same cluster or scatterers thus ensuring that the distances traveled by various multipath components (MPC)s are directly proportional to the time of their arrival and by extension their RMS DS at each small cells thus creating a linear distance dependency. The RMS DS distance dependency model is represented by (1):

$$RMS DS_{Street Canyon} = 0.4d + 25.41 \quad (1)$$

where d (meters) is the distance between BS-SC

In the case of the high-rise scenario, when we plot the simulation results of the RMS delay spread against the building height as shown in Figure 2, we noticed that the RMS DS of some set of small cells is relatively constant along with a range of height. For example, the RMS DS for small cells 7 to 15 (7th to 15th floors) lies between 60 ns – 90 ns while that for small cells 16 to 23 (16th to 23rd floors) lies between 200 ns – 240 ns. These can be explained by the observance of multiple arriving clusters where the MPCs of different

clusters arrived at a different set of small cells, with the MPCs of clusters 2 and 3 taking the longer route and thus longer delay time of arrival than MPCs of cluster 1. The multiple arriving clusters are due to the high-rise environment with reflections from low-rise and building rooftops. When we plot a fitting curve for the RMS DS distance dependency, we see a fairly strong positive association of the second-order polynomial. In our selection, we compared the second-order polynomial with the exponential where the R-square and the RMSE goodness of fit for the second-order polynomial were better than that of the exponential. The RMS DS increases with the height of the building as depicted by the fitted curve. The RMS DS distance dependency model for the high-rise is thus given by (2):

$$RMS\ DS_{Highrise} = 0.61x^2 - 6.99x + 100 \tag{2}$$

where x is the building floor number. Other authors have investigated the RMS DS distance dependency including the author of [21] where measurement based on a 4 x 4 FD-MIMO antenna system was performed and the RMS DS curve run in zigzag with the increase in distance as the fluctuation matches the changes of the street layouts in the LOS street canyon scenario.

This is because every point of the RMS DS was connected rather than a fitted curve. In our work, we would have obtained the same observation except that we used a fitted curve. Yu *et al.* [22] investigated the RMS DS distance dependency for small cells in indoor stair and corridor scenario where no linear relationship exist between the two quantities because the reflection and scattering of the NLOS environment level the relationship between distance and RMS DS. Other authors who worked on RMS DS and distance relationships include [23].

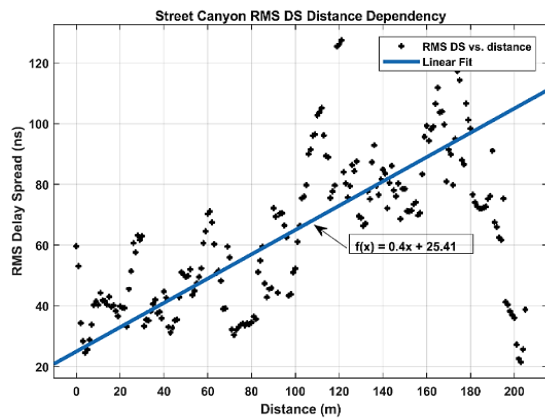


Figure 1. RMS DS DD model for street canyon

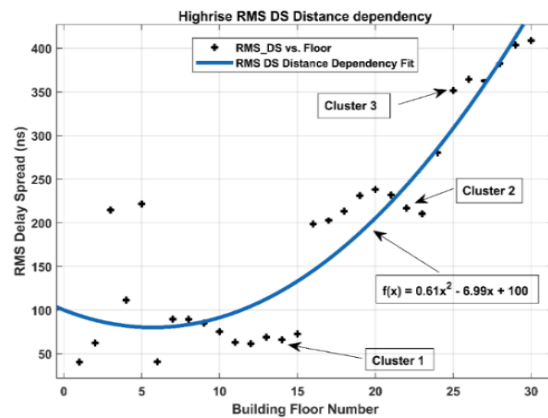


Figure 2. RMS DS DD model for high-rise

3.1.2. RMS delay spread modelling

Figure 3 shows the RMS DS distribution for the street canyon where we noticed a normal distribution with a mean of 40.89 and a standard deviation of 5.76. The arriving multipath components (MPCs) are from a single cluster. The distribution of RMS DS of the street canyon scenario follows a normal distribution and using the statistics of the distribution we obtain the model as shown in (3) [21].

$$f(DS)_{Street} = \frac{1}{\sigma_{DS}\sqrt{2\pi}} e^{-\frac{(DS - \mu_{DS})^2}{2\sigma_{DS}^2}} \tag{3}$$

In the case of the high-rise, however, we noticed a different observation where Figure 4 shows the RMS DS pdf distribution with significantly different characteristics from the street canyon scenario. The RMS DS has three peaks from three clusters, all of which are independent and well fitted by two different distributions. The first arriving cluster is modeled as a normal distribution with a mean of 69.05 and standard deviation of 20.63 and the second and third clusters are modeled as lognormal distribution with a mean and standard deviation of 5.387 and 0.099, 5.949, and 0.063 respectively. The distribution of the RMS DS for the first arriving cluster for the high-rise (normal distribution) can be modeled as shown in (3) using the statistics of the high-rise first arriving cluster. The second and third arriving clusters which are lognormal distribution can be modeled as shown in (4) where the statistics of the second arriving cluster can be replaced with the statistics of the third arriving cluster to obtain its model as shown in (4) [21].

$$f(DS)_{Highrise2} = \frac{1}{\sqrt{2\pi} \cdot \sigma_{DS HR2}} e^{-\frac{(\log_{10} DS_{HR2} - \mu_{DS HR2})^2}{2\sigma_{DS HR2}^2}} \quad (4)$$

Where HR_2 represents the second arriving cluster. It has been established that DS characteristics depend more on the propagation environment and the signal bandwidth than the carrier frequency [24]. The difference in our results for both scenarios is therefore as a result of the different environmental characteristics. Explaining the differences in the RMS DS result obtained, based on the different propagation environments, we noticed that broad street with a width of about 14 m having buildings of between 5 stories to 20 stories lining the sides create a waveguide for the transmitted signal causing a single clustered rays to reach all receivers. In the high-rise scenario, there is a disappearance of LOS rays and the arriving rays are predominantly from multiple reflections of surrounding high-rise buildings and low-rise buildings' rooftops. Rays or MPCs coming from such scatterers have entirely different propagation paths and thus arriving as independent rays. This is consistent with a dense high-rise environment [25]. It is seen that the values of the RMS delay spread for the high-rise scenario are much higher than the values for the street canyon scenario as shown in Table 1. This is as a result of the fact that the rays to the street small cells have LOS or near LOS propagation. On the contrary, the rays to the high-rise small cells follow predominantly NLOS directions which took a longer time to arrive as a result of the many reflectors or scatterers. It is thus expected that the symbol rate for the high-rise scenario may be higher than for the street scenario to mitigate intersymbol interference (ISI). According to WINNER+ [26], RMS delay spread of signals with small measurement bandwidth tends to be large and vice versa, it is thus understandable why our result with 100MHz bandwidth shows values smaller than what is obtained by WINNER+ with 10 MHz bandwidth as shown in Table 2.

Table 2. Comparison of RMS DS for street canyon and high-rise

	Street (ns)	W+ (ns)	High-rise (ns) O2I	W+ (ns) O2I
Min RMS DS	8.19	≈ 8	40.38	N/A
Max RMS DS	207.82	> 600	408.80	N/A
Mu (μ)	40.89	123.0	69.04, 5.39, 5.95	70.28
Sigma (σ)	5.76	73.2	20.63, 0.1, 0.06	43.51
pdf	Normal	Normal	Normal, Lognormal, Lognormal	Normal

W+ : is WINNER+

If we take the cumulative distribution function (CDF) of the RMS delay spread for the street canyon and high-rise as shown in Figures 5 and 6 respectively and then draw out the statistics as shown in Table 3, we see that most of the high valued RMS DS are from weak MPCs that do not contribute considerable energy to the received signal as the 90% CDF figure shows. For example for the street canyon scenario, 90% percentile gives 48 ns while the maximum figure is 207.82 ns (from Table 2). These results are useful for designing receivers with appropriate filters to cut off such MPCs with high RMS DS values.

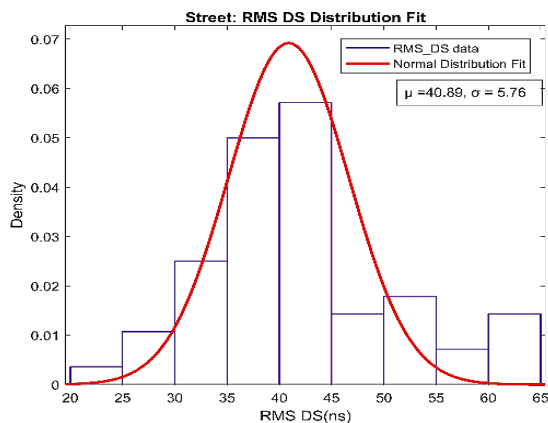


Figure 3. Distribution of RMS DS for street canyon

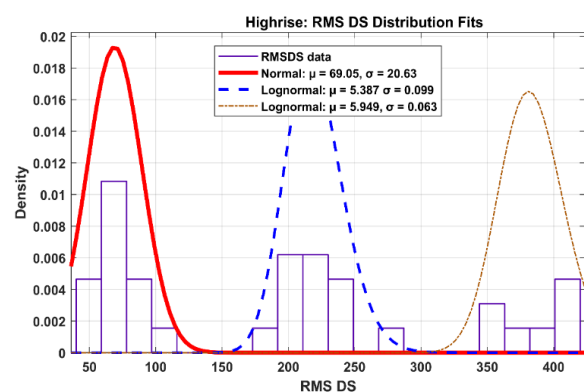


Figure 4. Distribution of RMS DS for high-rise

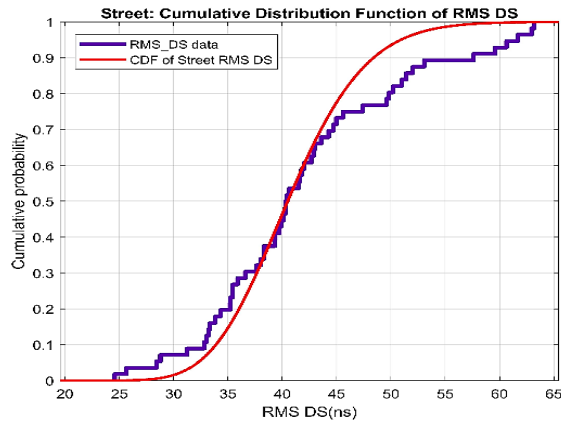


Figure 5. CDF for street canyon

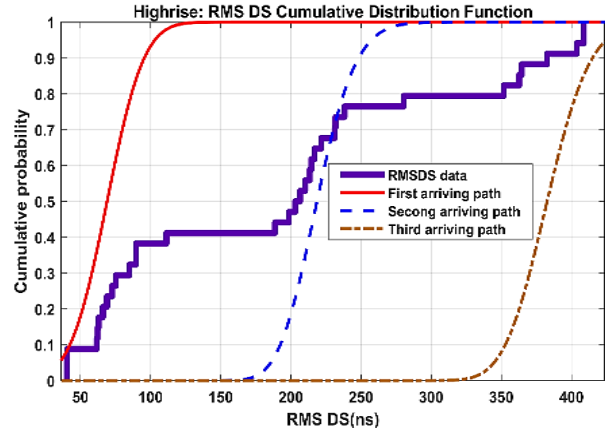


Figure 6. CDF for high-rise

Table 3. RMS delay spread statistics

	High-rise	Street	WINNER+
10% percentile	25ns, 190ns, 355ns	32.5ns	21.80ns
50% percentile	70ns, 215ns, 380ns	40ns	59.05ns
90% percentile	95ns, 250ns, 406ns	48ns	138.37ns

3.2. RMS angular spread

Wireless World Initiative New Radio WINNER+ Final Model D5.3_v1.0 [27] and the third generation partnership project (3GPP 3D) has been encouraged to include elevation parameters in their models and also provide accurate 3D channel models which are greatly helping to evaluate the potential of 3D MIMO techniques such as 3D beamforming and 3D sectorization. These 3D channel models are also helping researchers in providing answers to questions of particular interest such as the effect of distance on elevation spread, what is the impact of receiver height on elevation spread, what is the best modeling of elevation statistical distributions, and what impact does elevation spread has on channel capacity. These are part of the questions we make efforts to answer in this section.

3.2.1. RMS ESA/ESD distance dependency for street canyon

According to WINNER+, fixed elevation spread is assumed per environment irrespective of the distance of the receiver from the BS. However, based on an obtained dataset from our simulation, we observe that the elevation spread for both departure (ESD) and arrival (ESA) rays decreases as a function of distance from the BS for the street canyon scenario. When we plot the spread against distance in the elevation domain at the arrival, it becomes clear that there is a correlation pattern between the elevation spread and the BS-SC distance where the spread constantly decreases with distance as seen in Figure 7.

The same behavior is observed in the elevation domain at the departure in Figure 8. We may explain this observation as a result of the ground reflections of the elevation rays in LOS or near LOS situation where the movement of the UE/SC away from the BS causes a constant reduction in the angle between the reflection direction and the LOS/near LOS direction. Thus, the ESA and ESD which are based on the interplay of these angles are expected to decrease with the increase of the distances between the BS and small cells.

Modeling the RMS ESA distance dependency, we see an exponential relationship as depicted by the fitted exponential curve in Figure 8. The model is represented by (5).

$$f(x)_{RMS\ ESA} = 41.35e^{-0.15x} + 2.56 e^{-0.0025x} \tag{5}$$

Modeling the RMS ESD distance dependency, we see an exponential relationship as depicted by the fitted exponential curve in Figure 9. The model is represented by (6):

$$f(x)_{RMS\ ESD} = 28.93e^{-0.108x} + 0.436 e^{-0.0022x} \tag{6}$$

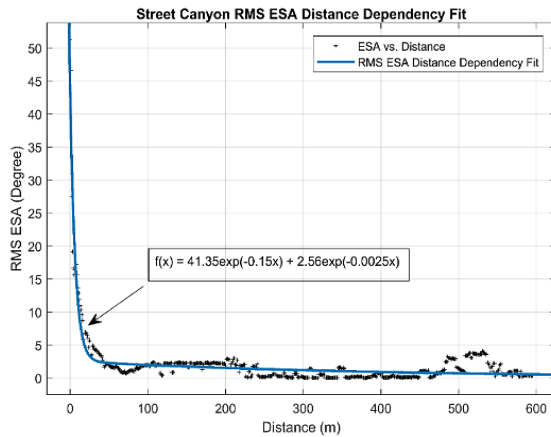


Figure 7. RMS ESA DD model for street canyon

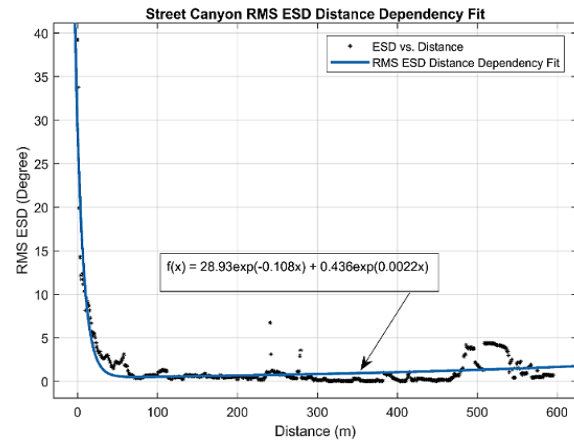


Figure 8. RMS ESD DD Model for street canyon

3.2.2. RMS ASA/ASD distance dependency for street canyon

Looking at the values of RMS ASA and RMS ASD corresponding to the incremental values of the distances from the BS to the small cells, it is difficult to observe any trend between the distance and ASA/ASD. A scatter plot for the two parameters with distance reveals a trend that cannot be explained via the ground reflection angles as seen in Figures 9 and 10. In trying to explain this observation in the azimuth domain, we first try to understand that AS does not pay much attention to the amount of incident power like the angular power spectrum but to the angular distribution. The values obtained for angular spread are a function of the arriving power via the most important MPC such as the LOS path divided by the power of the other MPCs arriving at the small cell in a much wider angular range.

If the power of the most significant MPC is much higher than the power of the scattered MPCs then the angular spreads would be small. However, if the scattered MPCs make a substantial input in the power spectra, the angular spreads will be large. Both figures show the zig-zag behavior of the RMS ASA/ASD as the distance increases. We explain this as follows. The small cells are spaced 1m apart along the street for high distance resolution observation and channel spatial consistency [28]. In the cases where the small cells along the street are within a closed corridor (without open feeder streets), the MPCs reflected from the walls have large power contributions in the incident power at the BS than the power contributed by the LOS MPC giving rise to a large angular spread. In the cases where the small cells along the street are within open spaces like feeder streets or open car parks, the MPCs scattered from the building walls will be weak and the contributed reflected power may be lower than the MPC power of the LOS component leading to smaller angular spread values. This explains the variations and fluctuations of ASA and ASD which matches the changes in the street structural construction and physical outlay.

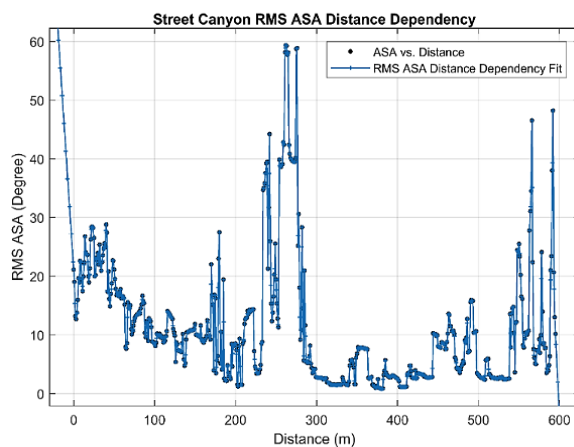


Figure 9. RMS ASA DD model for street canyon

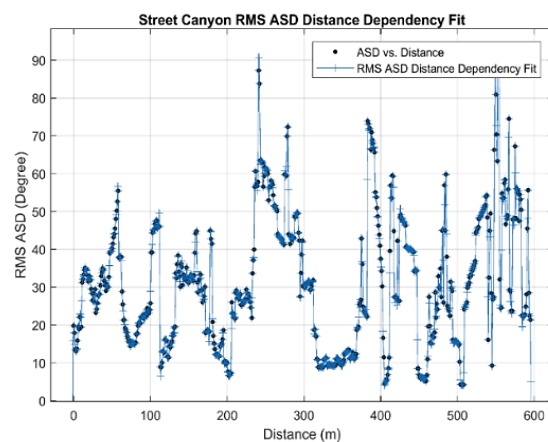


Figure 10. RMS ASD DD model for street canyon

3.2.3. RMS ESA/ESD distance dependency for high-rise

A close observation of the dataset reveals no trend for the low-rise up to the 3rd floor in both arrival and departure elevation spread, as the behavior is erratic. However, as we move through the medium-rise to high-rise floors (4th to the 30th floor), we noticed that rather than decrease, the elevation spread increases with height in both the arrival and departure. Modeling the RMS ESA distance dependency, we see a linear relationship as depicted by the fitted polynomial curve of the second order in Figure 11, where there is an increase of the elevation spread of arrival with the height of the building. This can be explained by the fact that ESA value is a ratio, an increasing value of ESA with the height of the building shows that the LOS MPCs in the first arriving cluster is much larger than the scattered NLOS MPCs. However, as the height increases the portion of the ratio contributed by the scattered NLOS becomes increasingly much larger than the portion contributed by the LOS component. This is obvious since the later arriving clusters traveled longer distances due to reflections from low-rise and medium-rise rooftops and other buildings leading to much scattered NLOS MPCs. The behavior of elevation spread of departure distance dependency follows the same situation as that of the spread of arrival as seen in Figure 12 where there is an increase in the RMS ESD as the height of the building increases due to the same line of argument. Increase in RMS ESD from each arriving cluster due to the increasing contribution of the non-line of sight component to the ratio of the value of ESD. The models for RMS ESA and RMS ESD in high-rise scenarios are represented by (7) and (8) respectively.

$$f(x)_{RMS\ ESA} = -0.005x^2 + 0.72x - 1.37 \tag{7}$$

$$f(x)_{RMS\ ESD} = 1.59x - 4.90 \tag{8}$$

Hong *et al.* [29] and Zhang *et al.* [30] have carried out research based on measurement in a similar scenario. Hong *et al.* [29] measured ESA and ESD where the BS was installed at the top of a three-story building (10.8 m antenna height). The receivers are located on the first to eight floors in another building 21.5 m away. Zhang *et al.* [30] has their antenna height at 20.46 m and receivers located 47.5 m away on five different floors. In both cases, the ESA and ESD were plotted against the BS–receiver height difference and the result shows a negative correlation as ESA and ESD decrease with the reduction of the BS–receiver height difference. Our result shows a positive correlation with height. This is because while they use a decreasing BS–receiver height difference, we plotted ESA and ESD with increasing receiver height.

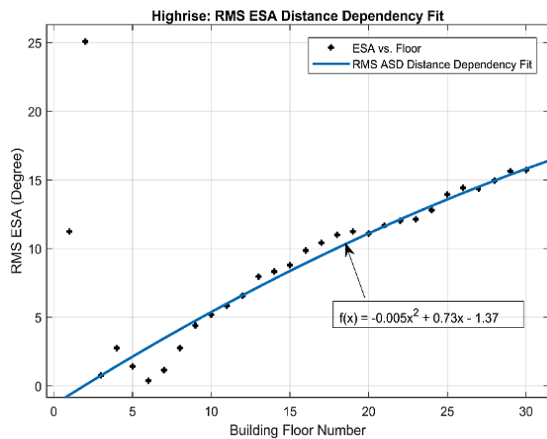


Figure 11. RMS ESA DD model for high-rise

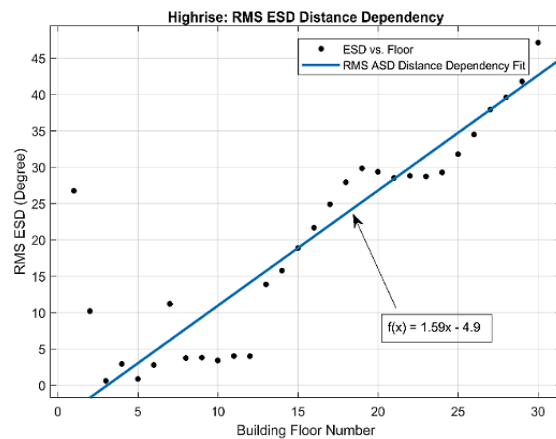


Figure 12. RMS ESD DD model for high-rise

3.2.4. RMS ASA/ASD distance dependency for high-rise

The RMS ASA distance dependency model shows a linear relationship as depicted by the fitted polynomial curve of the first order in Figure 13 where ASA decreases with distance unlike other parameters in the high-rise scenario that increases with height. This can be explained if we consider a decreasing value of ASA with the height of the building to mean that the LOS MPCs in the first arriving cluster are much smaller than the scattered NLOS MPCs since the lower part of the building is surrounded by dense low-rise building making LOS almost impossible.

However, as the height increases in the second and third arriving clusters, the portion of the ratio contributed by the scattered NLOS becomes increasingly smaller (as the major part of the building becomes visible) while the portion contributed by the LOS component becomes bigger. This is obvious since part of the transmitted beam is blocked by various close-by buildings in the first arriving cluster (this is evident in the small cells at the lower floors of the building being in an outage). Though later arriving clusters travel through longer distances with much scattered NLOS MPCs but their LOS MPCs at the arrival are much greater than their NLOS MPCs leading to a decreasing ASA as height increases. The RMS ASA model is given by (9).

$$f(x)_{RMS\ ASA} = -5.46x + 36.76 \tag{9}$$

The model of RMS ASD on the other hand increases with distance and is fitted by a polynomial curve of the first order as shown in Figure 14. The model is given by (10).

$$f(x)_{RMS\ ASD} = 1.076x + 21.44 \tag{10}$$

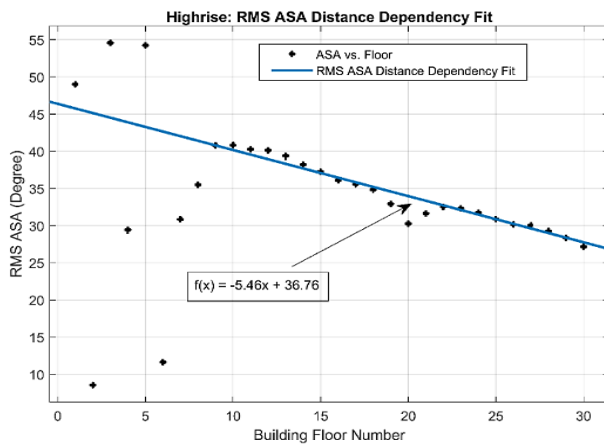


Figure 13. RMS ASA DD model for high-rise

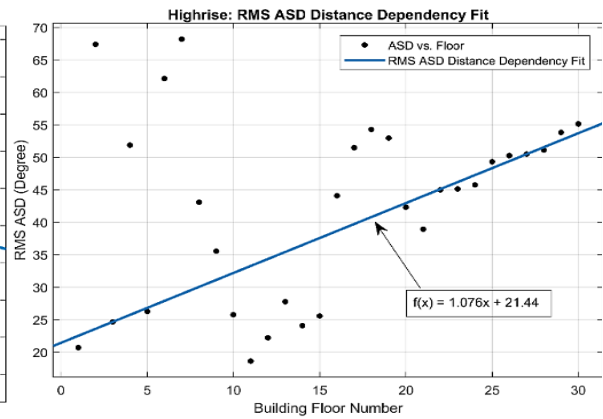


Figure 14. RMS ASD DD model for high-rise

3.2.5. Distribution of ESA and ESD

We collected 596 samples of ASA, ESA, ASD, and ESD for the street scenario and 30 samples for the high-rise scenario. These samples formed the sample sets for our curve fittings. The distributions of RMS ESA in the street canyon and high-rise scenarios are shown in Figures 15 and 16 respectively.

The RMS spread of arrival in the elevation domain for the street canyon and high-rise scenarios follows the lognormal distribution. With a lognormal distribution for RMS ESA in both scenarios. The mean and standard deviation of the two scenarios is given as street canyon (-0.24, 1.33) and high-rise (2.45, 0.20). The model for ESA for high-rise is shown in (11) while the model for the street canyon is given by (12) [21].

$$f_{ESA_{highrise}}(\theta) = \frac{1}{\theta \sigma_{ESA_{highrise}} \sqrt{2\pi}} e^{-\frac{(\ln \theta - \mu_{ESA_{highrise}})^2}{2\sigma_{ESA_{highrise}}^2}} \tag{11}$$

$$f_{ESA_{street}}(\theta) = \frac{1}{\theta \sigma_{ESA_{street}} \sqrt{2\pi}} e^{-\frac{(\ln \theta - \mu_{ESA_{street}})^2}{2\sigma_{ESA_{street}}^2}} \tag{12}$$

Where θ represents the elevation domain parameter, μ is the mean of the distribution and σ is the standard deviation.

The RMS spread of departure in the elevation domain for the street canyon and high-rise scenarios also followed the lognormal distribution. The model for the two scenarios is given by replacing the values of μ and σ for ESA high-rise and ESA street with ESD high-rise and ESD street values of μ and σ respectively in (11) and (12) where the mean and standard deviation of the two scenarios is given as street canyon (-0.51,

1.23) and high-rise (3.37, 0.08). Our observation in both scenarios follows the recommendation in WINNER+ where the RMS ESA spread is expected to be larger than the spread in ESD. For the street canyon scenario, ESA spread at 7° is larger than the spread in ESD at 5°. In the high-rise scenario, ESA spread at 15° is larger than ESD spread at 14°. This according to WINNER+ is because the UE moves at the street level which allows more scattering and reflection that lead to the increase in the angular spread.

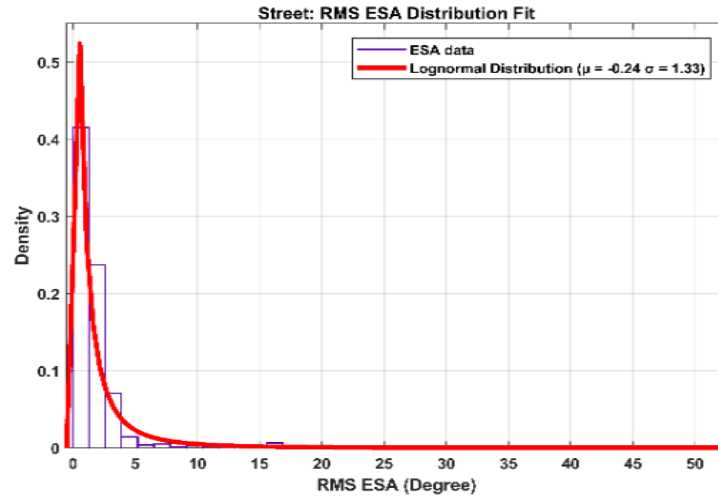


Figure 15. RMS ESA distribution for street canyon

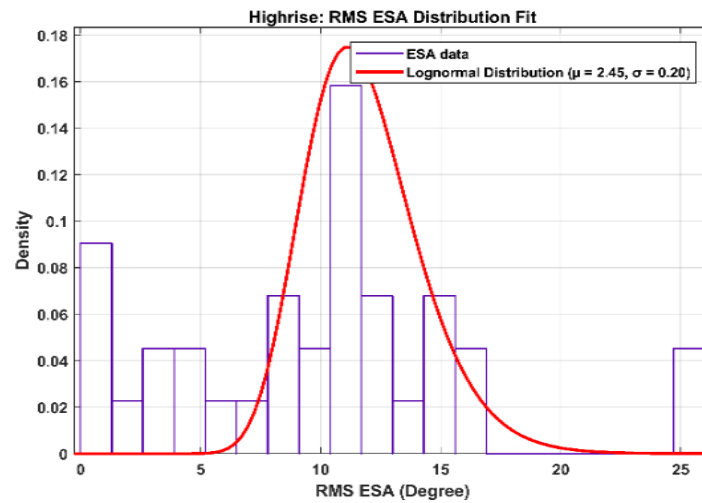


Figure 16. RMS ESA distribution for high-rise

3.2.6. Distribution of ASA and ASD

The distribution of RMS ASA in the street canyon and high-rise are shown in Figures 17 and 18 respectively. The RMS spread of arrival in the azimuth domain for both scenarios follows the lognormal distribution as recommended in WINNER+ with the mean and standard distribution of street canyon been 1.99 and 0.96 and that of high-rise been 3.50 and 0.12. The model for ASA for the high-rise can be represented by (13) while the model for the street canyon is given by (14) [21].

$$f_{ASA_{Highrise}}(\varphi) = \frac{1}{\varphi \sigma_{ASA_{highrise}} \sqrt{2\pi}} e^{-\frac{(\ln \varphi - \mu_{ASA_{highrise}})^2}{2\sigma_{ASA_{highrise}}^2}} \tag{13}$$

$$f_{ASA_{street}}(\varphi) = \frac{1}{\varphi\sigma_{ASA_{street}}\sqrt{2\pi}} e^{-\frac{(\ln \varphi - \mu_{ASA_{street}})^2}{2\sigma_{ASA_{street}}^2}} \tag{14}$$

Where φ represents the azimuth domain parameter.

The model for ASD for street canyon and high-rise is given by replacing the values of μ and σ for ASA high-rise and ASA street with ASD high-rise and ASD street values of μ and σ respectively in (13) and (14). The prediction by WINNER+ that the departure angular spread for the street scenario i.e., RMS ASD is smaller compared with the arrival angular spread i.e., RMS ASA is not observed. We noticed that the arrival spread at $\approx 45^\circ$ is smaller compared to the departure spread which is $\approx 90^\circ$ degrees. Similarly, the arrival spread for the high-rise at 24° is smaller than the departure spread at 50° . The reason for the above lies in the particular location of our BS which is located in an open space with a lot of high-rise buildings surrounding it in a concentric circle format. The BS is also below the surrounding buildings thus providing a rich scattering environment better than that at the arrival, leading to a high angular spread of departure as compared to the angular spread of arrival both at the street and high-rise scenarios. Unlike in the elevation domain where the departing rays met with little scatters allowing ESA to be greater than ESD, in the azimuth domain, the departing rays met with a lot of scatters leading to the situation where ASA is smaller than ASD.

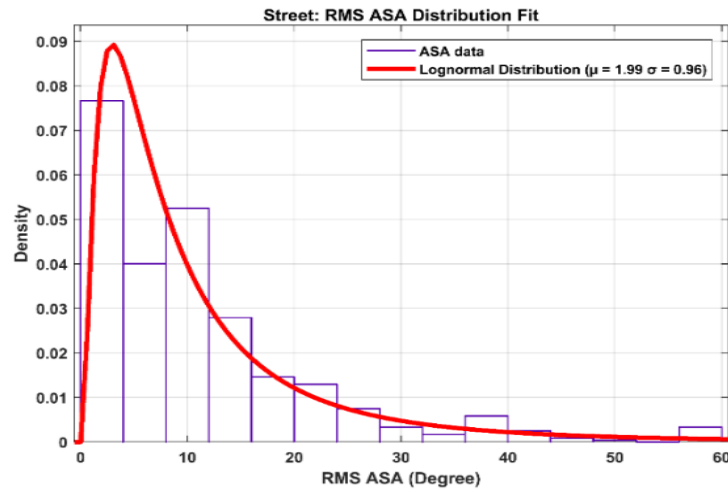


Figure 17. RMS ASA distribution for street canyon

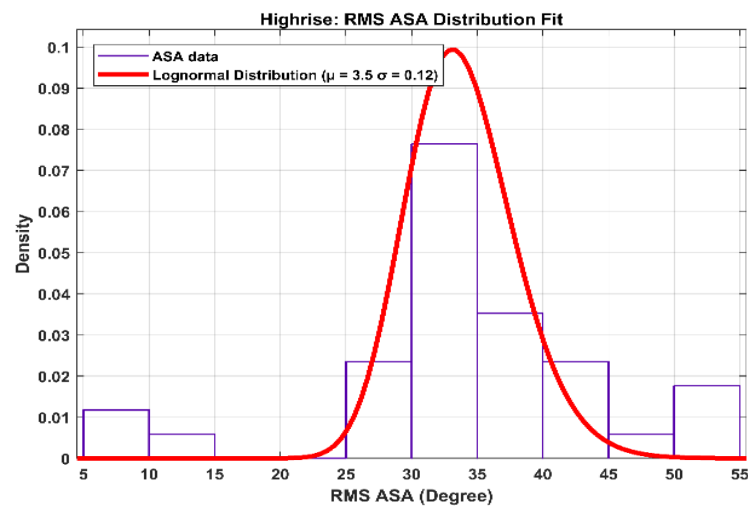


Figure 18. RMS ASA distribution for high-rise

3.3. Cross-correlation and statistics of large-scale parameters

Understanding the behavior of the parameters and their distribution functions is important, but the knowledge of the cross-correlation between them is also of pronounced interest and we can leverage this knowledge for more realistic channel simulations. In this contribution, the cross-correlation characteristics of the large-scale parameters in the spatial domain are investigated. The cross-correlation coefficient is key for analyzing the joint behavior of the parameters. To estimate the cross-correlation coefficients, all LSPs are usually distributed with certain values of the mean and the standard deviation from where the variance and covariance are derived. The cross-correlation coefficient between two different LSPs such as the ESD and ASD is then calculated as in (15) [21].

$$\rho = \frac{\text{cov}(X_{DS}, X_{ESA})}{\sqrt{\text{var}(X_{DS})\text{var}(X_{ESA})}} \quad (15)$$

Where $\text{cov}(\cdot)$ and $\text{var}(\cdot)$ are the covariance and variance of the given sequence(s) respectively. Table 4 is the result of our derived models and their correlation coefficients.

Table 4. Summary of the model's statistics for high-rise and street canyon scenarios

Parameter	Model statistics	Urban microcell environment	
		Street Canyon scenario	Urban high-density high-rise scenario
RMS DS [ns]	μ	40.89	69.04
	σ	5.76	20.63
RMS ESD[°]	μ	-0.51	3.27
	σ	1.23	0.22
RMS ASD[°]	μ	3.36	3.77
	σ	0.52	0.25
RMS ESA[°]	μ	-0.24	2.45
	σ	1.33	0.20
RMS ASA[°]	μ	1.99	3.50
	σ	0.96	0.12
CORRELATION			
RMS ESD vs RMS ASD		0.05	0.34
RMS ESA vs RMS ASD		-0.10	0.34
RMS ESD vs RMS ASA		0.17	-0.25
RMS ESA vs RMS ASA		0.14	-0.47
RMS ASD vs. RMS ASA		0.37	-0.80
RMS ESD vs RMS ESA		0.96	0.72
RMS DS vs RMS ASA		0.46	-0.10
RMS DS vs RMS ASD		0.58	0.35
RMS DS vs RMS ESA		-0.15	0.47
RMS DS vs RMS ESD		-0.10	0.77

4. CONCLUSION

This paper presented an insight into the behavior of large-scale parameters of the small cell backhaul link in UDN thereby solving the problem of the impact of small cell height on the new deployment scenario backhaul link. It was shown that the parameters increase with the height of the building except for RMS ASA that decreases, while RMS ESA/ESD for the street canyon decreases with distance, and the RMS ASA/ASD follows the structural construction of the environment. We also see the arrival of multiple clusters for the high-rise scenario. New sets of channel models for the backhaul link were presented. We conclude that site-specific models, that can factor in the impact of different propagation environments and terrains, offer a wide range of advantages when designing an efficient LTE cellular network. We intend to perform future simulations for city-wide coverage for better prediction.





ACKNOWLEDGEMENTS

This work was supported by the IoT-Enabled Smart and Connected Communities (SmartCU) Research Cluster of Covenant University, the Covenant University Centre for Research, Innovation, and Discovery (CUCRID), Nigeria, and REMCOM Corporation State College, PA 16801 USA.





REFERENCES

- [1] P. Zhang, C. Yi, B. Yang, C. X. Wang, H. Wang, and X. You, "In-building coverage of millimeter-wave wireless networks from channel measurement and modeling perspectives," *Science China Information Sciences*, vol. 63, no. 8, p. 180301, Aug. 2020, doi: 10.1007/s11432-019-2832-1.
- [2] A. H. Kelech, U. A. Samson, M. Simeon, O. Obinna, A. Alex, and A. A. Aderemi, "The quality of service of the deployed LTE technology by mobile network operators in Abuja-Nigeria," *International Journal of Electrical and Computer Engineering*, vol. 11, no. 3, pp. 2191–2202, 2021, doi: 10.11591/ijece.v11i3.pp2191-2202.
- [3] O. Idowu-Bismark, O. Kennedy, R. Husbans, and M. Adedokun, "5G wireless communication network architecture and its key enabling technologies," *International Review of Aerospace Engineering*, vol. 12, no. 2, pp. 70–82, Apr. 2019, doi: 10.15866/irease.v12i2.15461.
- [4] O. Idowu-Bismark, F. Idachaba, and A. Atayero, "Massive MIMO channel characterization and modeling: the present and the future," *International Journal of Applied Engineering Research ISSN*, vol. 12, no. 23, pp. 973–4562, 2017.
- [5] O. Idowu-Bismark, F. Idachaba, and A. A. A. Atayero, "A survey on traffic evacuation techniques in internet of things network environment," *Indian Journal of Science and Technology*, vol. 10, no. 33, pp. 1–11, Sep. 2017, doi: 10.17485/ijst/2017/v10i33/112749.
- [6] O. Idowu-Bismark, O. Oyeleke, A. A. Atayero, and F. Idachaba, "5G small cell backhaul: A solution based on GSM-Aided hybrid beamforming," *International Journal of Computer Network and Information Security*, vol. 11, no. 8, pp. 24–31, Aug. 2019, doi: 10.5815/ijcnis.2019.08.03.
- [7] X. Zhao *et al.*, "Playback of 5G and beyond measured MIMO channels by an ANN-Based modeling and simulation framework," *IEEE Journal on Selected Areas in Communications*, vol. 38, no. 9, pp. 1945–1954, Sep. 2020, doi: 10.1109/JSAC.2020.3000827.
- [8] 3GPP TR 38.901, "TR 138 901 - V15.0.0 - 5G; Study on channel model for frequencies from 0.5 to 100 GHz (3GPP TR 38.901 version 15.0.0 Release 15)," *3Gpp*, 2017. [Online]. Available: <http://www.etsi.org/standards-search>. Accessed July 10, 2020
- [9] J. Medbo *et al.*, "Radio propagation modeling for 5G mobile and wireless communications," *IEEE Communications Magazine*, vol. 54, no. 6, pp. 144–151, Jun. 2016, doi: 10.1109/MCOM.2016.7498102.
- [10] T. L. Nguyen and D. T. Do, "Investigation on energy harvesting enabled device-to-device networks in presence of co-channel interference," *Telkomnika (Telecommunication Computing Electronics and Control)*, vol. 19, no. 1, pp. 27–35, Feb. 2021, doi: 10.12928/TELKOMNIKA.V19I1.16138.
- [11] Y. J. Cho, G. Y. Suk, B. Kim, D. K. Kim, and C. B. Chae, "RF lens-embedded antenna array for mmWave MIMO: Design and performance," *IEEE Communications Magazine*, vol. 56, no. 7, pp. 42–48, Jul. 2018, doi: 10.1109/MCOM.2018.1701019.
- [12] Y. G. Lim, T. Jung, K. S. Kim, C. B. Chae, and R. A. Valenzuela, "Waveform multiplexing for new radio: Numerology management and 3D evaluation," *IEEE Wireless Communications*, vol. 25, no. 5, pp. 86–94, Oct. 2018, doi: 10.1109/MWC.2018.1700351.
- [13] M. K. Samimi and T. S. Rappaport, "3-D millimeter-wave statistical channel model for 5G wireless system design," *IEEE Transactions on Microwave Theory and Techniques*, vol. 64, no. 7, pp. 2207–2225, Jul. 2016, doi: 10.1109/TMTT.2016.2574851.
- [14] V. Nurmela *et al.*, "Deliverable D1.4 METIS channel models," *METIS Channel Models*, 205AD, 2015. https://metis2020.com/wp-content/uploads/deliverables/METIS_D1.4_v1.0.pdf (Accessed Jan. 18, 2021).
- [15] Z. Gao, L. Dai, D. Mi, Z. Wang, M. A. Imran, and M. Z. Shakir, "MmWave massive-MIMO-based wireless backhaul for the 5G ultra-dense network," *IEEE Wireless Communications*, vol. 22, no. 5, pp. 13–21, Oct. 2015, doi: 10.1109/MWC.2015.7306533.
- [16] W. Xia *et al.*, "Millimeter wave channel modeling via generative neural networks," *2020 IEEE Globecom Workshops, GC Wkshps 2020 - Proceedings*, 2020, doi: 10.1109/GCWkshps50303.2020.9367420.
- [17] R. N. Almesaedi, A. S. Ameen, E. Mellios, A. Doufexi, and A. Nix, "3D channel models: Principles, characteristics, and system implications," *IEEE Communications Magazine*, vol. 55, no. 4, pp. 152–159, Apr. 2017, doi: 10.1109/MCOM.2017.1500505.
- [18] M. Yang *et al.*, "Measurements and cluster-based modeling of vehicle-to-vehicle channels with large vehicle obstructions," *IEEE Transactions on Wireless Communications*, vol. 19, no. 9, pp. 5860–5874, Sep. 2020, doi: 10.1109/TWC.2020.2997808.
- [19] M. H. Alsharif, K. Yahya, and S. A. Chaudhry, "Analyzing and evaluating the energy efficiency based on multi-5G small cells with a mm-waves in the next generation cellular networks," *International Journal of Electrical and Computer Engineering*, vol. 10, no. 4, pp. 3492–3500, Aug. 2020, doi: 10.11591/ijece.v10i4.pp3492-3500.
- [20] Q. Zheng, J. Zhang, H. Yu, Y. Zhang, and L. Tian, "Propagation statistic characteristic of 3D MIMO channel in outdoor-to-indoor scenario with different antenna heights," *International Symposium on Wireless Personal Multimedia Communications, WPMC*, pp. 411–416, 2017.
- [21] R. Zhang, X. Lu, J. Zhao, L. Cai, and J. Wang, "Measurement and modeling of angular spreads of three-dimensional urban street radio channels," *IEEE Transactions on Vehicular Technology*, vol. 66, no. 5, pp. 3555–3570, 2017, doi: 10.1109/TVT.2016.2604394.
- [22] Y. Yu, Y. Liu, W. J. Lu, and H. B. Zhu, "Measurement and empirical modelling of root mean square delay spread in indoor femtocells scenarios," *IET Communications*, vol. 11, no. 13, pp. 2125–2131, Sep. 2017, doi: 10.1049/iet-com.2017.0410.
- [23] Z. R. Wen *et al.*, "Measurement and Modeling of LTE-Railway channels in high-speed railway environment," *Radio Science*, vol. 55, no. 4, Apr. 2020, doi: 10.1029/2019RS007050.
- [24] P. F. M. Smulders and L. M. Correia, "Characterisation of propagation in 60 GHz radio channels," *Electronics and Communication Engineering Journal*, vol. 9, no. 2, pp. 73–80, Apr. 1997, doi: 10.1049/ecej:19970204.
- [25] X. Y. Wang, B. Li, X. Yuan, J. W. Dou, and Y. Li, "Elevation angle research in three-dimension channel model using ray-tracing," in *2014 31th URSI General Assembly and Scientific Symposium, URSI GASS 2014*, Aug. 2014, pp. 1–4, doi: 10.1109/URSIGASS.2014.6929281.
- [26] J. Meinil, I. Reseacher, P. Ky, H. Technologies, and N. Sad, "CP5-026 WINNER+ D5.3 v1.0 WINNER+ Final Channel Models," *Eurescom, Heidelberg, Germany, Technical Report*, no. May 2016, pp. 0–107, 2010.
- [27] J. Meinilä, *et al.*, "D5. 3: WINNER+ Final Channel Models V1. 0," *Article (CrossRef Link)*, vol. 5, no. 107, pp. 1–107, 2010.
- [28] Y. Lim, Y. J. Cho, M. Sim, Y. Kim, C.-B. Chae, and R. A. Valenzuela, "Map-based millimeter-wave channel models: An overview, hybrid modeling, data, and learning," *arxiv*, pp. 1–10, Nov. 2017, [Online]. Available: <http://arxiv.org/abs/1711.09052>.
- [29] Q. Hong *et al.*, "The impact of antenna height on 3D channel: A ray launching based analysis," *Electronics (Switzerland)*, vol. 7, no. 1, p. 2, Jan. 2018, doi: 10.3390/electronics7010002.
- [30] R. Zhang, X. Lu, W. Duan, L. Cai, and J. Wang, "Elevation domain channel measurement and modeling for FD-MIMO with different UE height," in *2015 IEEE Wireless Communications and Networking Conference, WCNC 2015*, Mar. 2015, pp. 70–75, doi: 10.1109/WCNC.2015.7127447.





BIOGRAPHIES OF AUTHORS

Olabode Idowu-Bismark     is currently a Ph.D. student at Covenant University, Ota, Nigeria. He holds an M.Sc degree in Telecommunications Engineering from Birmingham University UK in 2014 and a B.Eng. Electrical and Electronics Engineering from the University of Benin, Nigeria in 1990. Olabode is a ZTE University China certified RF engineer and a certified Optical Fiber/Transmission engineer, he has worked in various companies including Logic Sciences Limited and Primotek Systems Limited as an engineer, senior engineer, and technical manager. He is a member of the Nigerian Society of Engineers and IEEE, his research interest is in the area of mobile communication, mmWave, and MIMO communication. He has published many scientific papers in international peer-reviewed journals and conferences. He can be contacted at email: idowubismarkolabode@gmail.com, olabode.idowu-bismark@stu.cu.edu.ng.



Prof. Francis E Idachaba     is currently a Professor of Communication Engineering in the Department of Electrical and Information Engineering at Covenant University Ota Ogun State. He obtained his Ph.D. in Electronics and Telecommunication Engineering from the University of Benin in Edo State Nigeria. With over 15 years in academia, he has within the last five years served as a research fellow in 2013 at the Massachusetts Institute of Technology in the US. He has over 90 publications in both journals and conferences. He is actively involved in the Internet of Things Research, 5G communications research, and Smart Cities Research among other interests. He is a member of the Society of Petroleum Engineers, the Nigerian Society of Engineers, and a Registered Engineer in Nigeria. He can be contacted at email: rancis.idachaba@covenantuniversity.edu.ng.



Prof. Aderemi Atayero     is The Covenant University Professor of Communication Engineering. He has a Bachelor of Science Degree in Radio Engineering and a Master of Science Degree in Satellite Communication Systems in 1992 and 1994 respectively. He earned his Ph.D. from the Moscow State Technical University of Civil Aviation (MSTUCA) in 2000. Atayero is a Fellow of the Science Association of Nigeria (FSAN) as well as a Senior Research Fellow of the International Association of Research Scholars and Administrators. Engineer Atayero is a COREN Registered Engineer and member of the Institute of Electrical and Electronics Engineers (IEEE). He has published over a hundred scientific papers in both journals and conferences. His current research interests are in various aspects of Communication Engineering, including Wireless Sensor Networks, Wireless (Mobile) Communications, Internet of Things (IoT), Smart Cities, and Cyber-Physical Systems. He can be contacted at email: atayero@covenantuniversity.edu.ng.